JTTEE5 20:328–335
DOI: 10.1007/s11666-010-9550-8
1059-9630/$19.00 © ASM International

Analysis of the Mechanical Properties of an Arc-Sprayed WC-FeCSiMn Coating: Nanoindentation and Simulation

W. Tillmann, B. Klusemann, J. Nebel, and B. Svendsen

(Submitted April 28, 2010; in revised form July 28, 2010)

The characterization of thermal-sprayed coatings is often limited to microstructural analysis to evaluate the coatings morphology. Indentation is commonly used to determine the mechanical properties of different kinds of engineering materials. However, due to the complex structure of thermal-sprayed coatings, few results have been obtained so far. In this article, experimental nanoindentation tests and simulation results are compared. The experimental indentation tests show scattering in the force-deformation data due to the complex structure of the arc-sprayed coating which is investigated by means of an indentation test simulation. Based on the results for single constituent parts of the coating, the Young's modulus as well as further mechanical properties are identified. A general procedure is presented to predict the effective mechanical properties based on the microstructure, porosity, chemical composition, and properties of the coating after thermal spraying.

Keywords arc-spraying, image processing, material properties, microstructure, nanoindentation, simulation

1. Introduction

Arc-sprayed deposits are increasingly being used in a wide variety of industries. In order to understand, predict, and improve the reliability of coated devices, it is necessary to characterize their mechanical properties. The determination of the mechanical properties in thermal-sprayed coatings is quite complicated, and often contradictory mechanical properties are reported. Santana et al. (Ref 1) reported the Young's modulus of HVOF-sprayed WC-12Co to be 268 GPa. This property was determined by depth-sensing micro-indentation using the method proposed by Oliver and Pharr (Ref 2, 3). Ghafouri-Azar et al. (Ref 4) investigated also a coating of WC-12Co type, deposited by HVOF spraying, regarding residual stresses. They used a Young's modulus of 669 GPa in the simulation, which is nearly three times higher than the value reported in Ref 1. Toparli et al. (Ref 5) used a Young's modulus of 398 GPa for HVOF thermally sprayed WC-Co material in their simulation. This value originates from Delfosse et al. (Ref 6), who reported elastic-plastic properties for different WC-Co composites. However, these values were determined for materials manufactured by powder metallurgical process, involving several high pressure and high temperature treatments. Also Hussainova et al. (Ref 7) reported the mechanical properties of WC-Co composites, fabricated by conventional PM technology. The Young's modulus values determined by them using Vickers indentation for WC-8Co and WC-15Co were 650 and 560 GPa, respectively. These different reported values show the complexity of determination of mechanical properties of composites like WC-Co, thermal sprayed, as well as powder metallurgy fabricated. It is to be noted that the microstructural aspects of coatings are different from bulk materials which can lead to unexpected mechanical behavior as well as different mechanical properties (Ref 8, 9).

In this research study, a twin wire arc spraying (TWAS) facility (Smart Arc PPT 350, Sulzer Metco, Switzerland) was employed to spray WC-FeCSiMn coatings. The work principle of the spraying process is described elsewhere (Ref 10-12). The Duramat AS 850 flux-cored wire with a diameter of 1.6 mm (Durum GmbH, Germany) was used as wire feedstock material. The wire is Fe-based alloyed with 2 wt.% C, 1.4 wt.% Si, and <1 wt.% Mn. It is filled with 50 wt.% of fused tungsten carbide (WC/W_2C) with grain sizes of 25-125 μm. Based on the parameter optimization presented in Ref 12, the coatings were sprayed on grit blasted and cleaned medium carbon steel specimens (Mat. No. 1.0503, DIN

This article is an invited paper selected from presentations at the 2010 International Thermal Spray Conference and has been expanded from the original presentation. It is simultaneously published in *Thermal Spray: Global Solutions for Future Applications, Proceedings of the 2010 International Thermal Spray Conference*, Singapore, May 3-5, 2010, Basil R. Marple, Arvind Agarwal, Margaret M. Hyland, Yuk-Chiu Lau, Chang-Jiu Li, Rogerio S. Lima, and Ghislain Montavon, Ed., ASM International, Materials Park, OH, 2011.

W. Tillmann and **J. Nebel**, Institute of Materials Engineering, Dortmund University of Technology, Leonhard-Euler-Str. 2, 44227 Dortmund, Germany; and **B. Klusemann** and **B. Svendsen**, Institute of Mechanics, Dortmund University of Technology, Leonhard-Euler-Str. 5, 44227 Dortmund, Germany. Contact e-mails: wolfgang.tillmann@udo.edu, benjamin.klusemann@udo.edu and jan.nebel@udo.edu.

C45, AISI 1045) applying a voltage of 30 V, a current of 220 A, and an atomization gas pressure of 6 bar with a spraying distance of 100 mm.

For the investigated WC-FeCSiMn coating, no material properties are available in the literature. Therefore, the determination of mechanical properties either from direct measurements or parameter identifications are focused in this article. This helps us to understand their behavior during forming processes much better. In general, as a first assumption, it can be anticipated that the properties are similar to WC-Co composites due to the similar mechanical properties of Co and Fe as binder. However, in WC-Co the wt.% of WC is often above 80%, whereas the composite investigated here contains approximately 50% Fused Tungsten Carbide (FTC).

As reported in the literature (Ref 13-15), the material properties of thermally sprayed coatings are different in tension and compression. Conventional test procedures like bending and tensile tests are too complicated to realize on coatings (Ref 11). To determine mechanical properties of coatings, nanoindentation technique has been established. However, the strain fields under an indenter are complex, and the analysis of data is non-trivial especially for complicated material systems like thermally sprayed coatings. A disadvantage of using nanoindentation for inhomogeneous materials to identify the mechanical properties is that only local properties could be determined. These local properties have to be identified for each single material phase which can then be used to approximate the effective mechanical properties with the help of micrographs and different homogenization techniques as described later. Another possibility is to perform a number of nanoindentation tests and to determine the average value of the obtained results to realize the effective properties. However, a large number of tests are necessary to obtain reliable results.

The focus of this article is the application of a method to identify the mechanical properties (elastic and inelastic) of an arc-sprayed coating with the help of nanoindentation technique, finite element modeling, and homogenization methods.

2. Nanoindentation

2.1 Experiment

The nanoindentation experiments were performed using a Nanoindenter XP with Berkovich tip (MTS Nano Instruments, Oak Ridge, TN, USA) at the Institute of Materials, Ruhr University Bochum. Two sets of experiments were performed where the indenter either penetrated the polished coating in its normal direction or a polished cross section (see Fig. 1). The indentation was carried out at 49 points in a regular pattern for three indentation depths (100, 250, and 500 nm). Figure 1 shows an overview of the indentations into a cross section of the coating for a depth of 100 nm. As the chemical composition of an indented material is not known a priori, the indentations were analyzed in the Scanning Electron

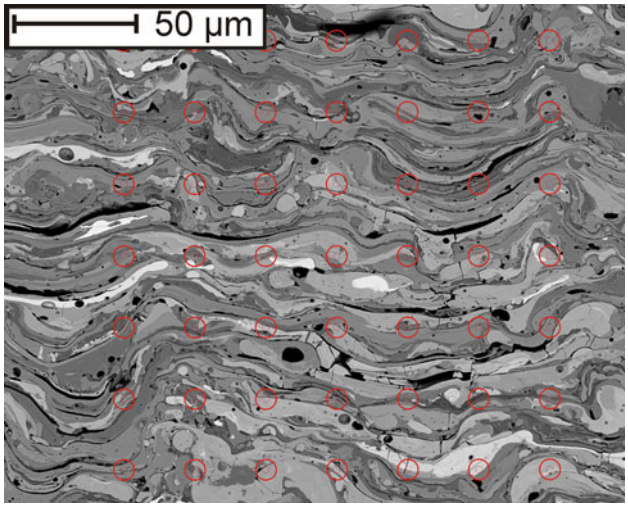

Fig. 1 Overview of indentations for a depth of 100 nm—TWAS WC-FeCSiMn coating

Microscope (SEM) employing EDX afterward, to identify, respectively, which phase was indented and which points have a chemical composition with a mass percentage of one of the constituents being above 80% for FTC and 80% for FeCSiMn. Only those indentations wherein one single phase without pores and cracks was indented were considered. Therefore, a large amount of indentations are necessary to indent in certain single phases. Investigations of the micrographs of the coating show that phases of different compositions can be identified because of the material contrast in the back-scattering mode of the SEM. However, it has to be mentioned that no quantitative separation, e.g., between WC and W_2C, could be made. This also implies that it cannot be identified which phase combinations (i.e., FeCSiMn) are generated during the thermal-spraying process. This could be the one reason for the deviations that were obtained between the load-displacement curves at different sample points with nearly the same chemical composition. Another reason for these deviations could also be the different residual stresses at different locations. It is anticipated that the indentation depth is small compared to the thickness of one single lamella and that the results found for one chemical composition only represent the behavior of this specific composition. This assumption is not valid for indentation into the coating surface due to the smaller thickness of the lamellas in this direction. Therefore, the following procedure is based on the results of the nanoindentation test into cross sections. Figures 2 and 3 show exemplary back-scattered electron images of indentation imprints into the coating as well as the corresponding EDX results into nearly pure FTC composition (Fe $<$ 20 wt.%) and FeCSiMn alloy (FTC $<$ 20 wt.%). As it can be seen from the EDX analysis, different pseudo-alloy combinations do exist.

The Young's modulus E is one of the most important mechanical properties. It describes the relation between stresses and strains in the elastic region. Nanoindentation can be used to determine the Young's modulus by

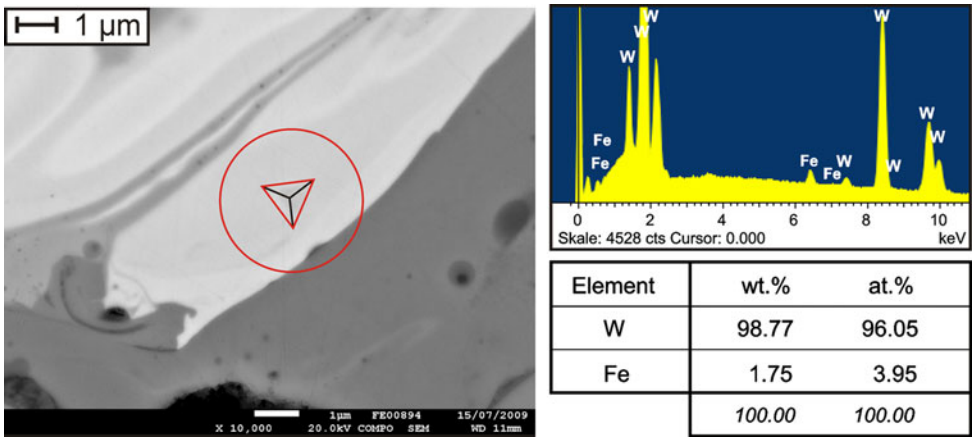

Element	wt.%	at.%
W	98.77	96.05
Fe	1.75	3.95
	100.00	*100.00*

Fig. 2 Detail view of analyzed point of indentation into FTC for a depth of 100nm and corresponding EDX analysis

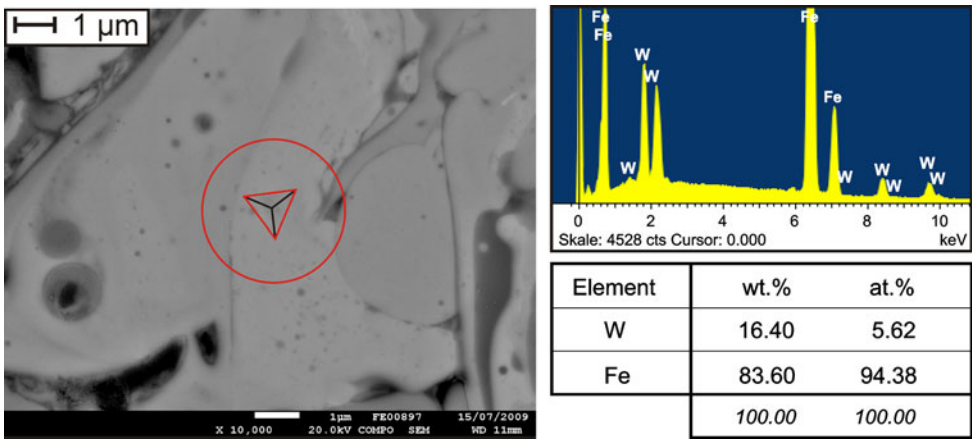

Element	wt.%	at.%
W	16.40	5.62
Fe	83.60	94.38
	100.00	*100.00*

Fig. 3 Detail view of analyzed point of indentation into FeCSiMn for a depth of 100 nm and corresponding EDX analysis

analyzing the unloading part of the load-displacement curve (Ref 16). The analysis and determination of the Young's modulus is performed with the traditional Oliver-Pharr (OP) method (Ref 2, 3, 11) at the corresponding unloading curves originating from an indentation into either pure FTC (<20 wt.% Fe) or FeCSiMn (<20 wt.% FTC). The Poisson ratio is chosen with respect to the bulk material, and therefore assumed for FTC composition as $\nu = 0.19$ and for the FeCSiMn alloy as $\nu = 0.3$ (Ref 17). The evaluated Young's moduli based on indentation into cross sections for a depth of 100 nm for the FTC and FeCSiMn phase are reported in Table 1. The averaged Young's moduli over all the 49 indents in cross sections as well as at the surface for the different indentation depths are reported in Table 2. As shown in the table, the Young's modulus is decreasing with increasing depth. One assumption for this is that the depth and, therefore, the loads are already too high, and failure occurs in the coating which affects the results. Therefore, mainly the results for a depth of 100 nm are used where it can be assumed that no or at least a minimum of failure occurs which makes the load-displacement curves and the obtained properties to be more reliable.

Table 1 Identified mechanical properties of single chemical composition for AS-850

Material	E, GPa	σ_0, MPa
FeCSiMn (<20 wt.% FTC)	190 ± 30	1900 ± 500
FTC (<20 wt.% FeCSiMn)	340 ± 40	4900 ± 600
	σ_{sat}, MPa	η_0
FeCSiMn (<20 wt.% FTC)	2650 ± 700	4.8 ± 1.5
FTC (<20 wt.% FeCSiMn)	6100 ± 700	60 ± 5.0

2.2 Finite Element Modeling of Nanoindentation

As mentioned in the previous section, several analytic methods are available to determine the Young's modulus. However, limited studies are available to obtain the plastic properties with the nanoindentation technique, e.g., Ref 18, 19.

Therefore, the indentation loading process is simulated by a finite element model with the software ABAQUS. The coating is modeled with continuum elements consisting of 8 nodes where the coating is modeled as

Table 2 WC-FeCSiMn Young's moduli for compression stresses

	Unit (method)	Mean Young's modulus	Young's modulus deviation
Indentation in surface	GPa (NanoIndent. 500 nm)	127	59
	GPa (NanoIndent. 250 nm)	142	37
	GPa (NanoIndent. 100 nm)	154	34
Indentation in cross section	GPa (NanoIndent. 500 nm)	165	31
	GPa (NanoIndent. 250 nm)	203	52
	GPa (NanoIndent. 100 nm)	240	70
Indentation simulation	GPa (NanoIndent. 100 nm) in surface	230	5
	GPa (NanoIndent. 100 nm) in cross section	212	4

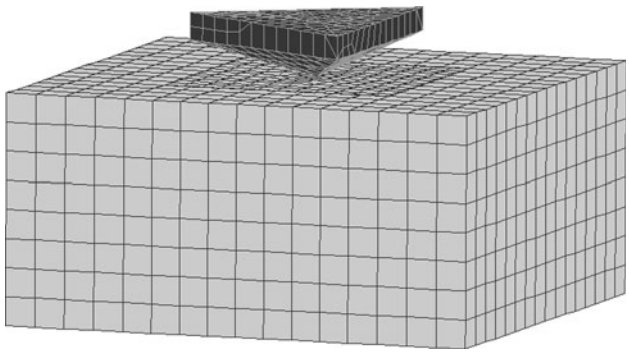

Fig. 4 Finite element mesh of indenter and coating

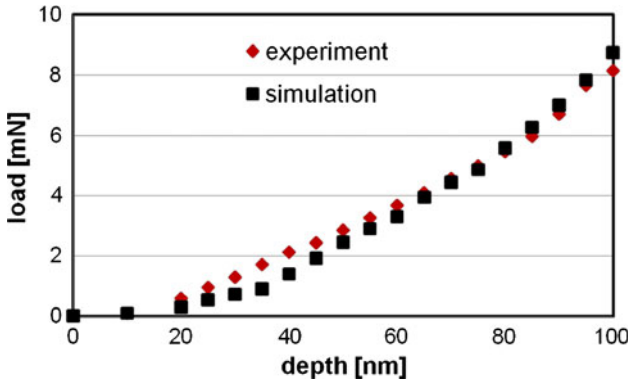

Fig. 5 Comparison between experimental and simulation data for indentation into FTC and an indentation depth of 100 nm

consisting of one single phase. The influence of the neighboring lamella on the mechanical behavior of the indented region is assumed to be negligible, so that only the indented material (lamella) is modeled. This is considered to be reasonable because of the small indentation depth when comparing with thickness of different material layers (cp. Fig. 1) which leads only to loading in one phase. Therefore, the modeling of the substrate is skipped. The indenter is modeled with rigid shell elements of the type R3D4. The surfaces of the coating as well as the indenter are defined as contact areas. Variation of the friction coefficient did not influence the obtained results as was previously mentioned also by other authors, e.g., Shan and Sitaraman (Ref 20). For this reason, the simulation is performed frictionless. The size of the modeled region is chosen in such a way that the stresses vanish at the free faces. The Finite element model is shown in Fig. 4.

In this study, the behavior of the material used is assumed to accord with type Voce hardening law given by

$$\sigma = \sigma_0 + (\sigma_{sat} - \sigma_0)\{1 - \exp(-\alpha_p n)\}, \quad \text{(Eq 1)}$$

where σ_0 describes the initial yield stress, σ_{sat} the saturation value of the stress, and n defines the rate at which the size of the yield surface changes as plastic straining develops, and α_p is the equivalent plastic strain.

The unknown material properties in (1) are identified using inverse finite element analysis method by fitting the simulation results to the experimentally obtained load-displacement curves. This determination is carried out using the program LS-OPT in conjunction with ABAQUS. The optimization techniques used rely on response surface methodology (RSM) (Ref 21), a mathematical method for constructing smooth approximations of functions in a design space. The approximations are based on results calculated at numerous points in the multi-dimensional design space. In this study, the material parameters are the design variables, and the model together with the data determines the objective function of the corresponding optimization problem. The material parameters that lead to the best fitting agreement can be considered to represent the constitutive behavior of the coating. Such a fit is shown in Fig. 5.

To find the material parameters, first a range for the design variables has to be defined. As initial values, the plastic properties of WC-Co are chosen from Ref 7. The simulation model and optimization method were first tested on results reported in Ref 22 for a steel coating. The identified material parameters agreed quite well with the reported one, so that the method presented as well as the simulation model seems to be justified. Based on the optimization history for one of the constituents, it can be observed that after some iteration steps, the LSOPT specific optimization borders are converging to one resulting value which describes the best fitting parameter for the problem. Table 1 displays the identified material parameters of the nanoindenter tests for the two phases. Figure 5 shows exemplarily the simulated load curve on top of the experimental one for indentation into FTC for an indentation depth of 100 nm.

It is worth mentioning that these parameters varied, depending on the position analyzed and the associated experimental data. The values displayed in Table 1 are

estimated from results of more than four points each for every phase. The deviation for the Young's modulus was app. 15%. The deviation for the plastic properties was app. 25%. These deviations occur from the inhomogeneities inside the coating. Therefore, the measured data describe only local properties at the microscale. To achieve the macro-properties like the effective Young's modulus, homogenization techniques are used which are described in the next section.

3. Construction of Finite Element Models from Real Micrographs

To perform analysis of real microstructures, micrographs of the thermal-sprayed coating were observed with different optical microscopes. As mentioned before, SEM micrographs served as a basis for the determination of the chemical composition of different phases. The micrograph enables us to distinguish between the phases because of the contrast in the brightness in the micrographs coming from regions with atoms having different atomic numbers. Correlating to the huge difference between the relative atomic weight of tungsten (183.84 g/mol) and that of iron (55.845 g/mol), the phases of the sprayed WC-FeCSiMn present features of a good contrast. In addition to these two phases, many pseudo-alloyed splats containing WC as well as FeCSiMn are visible which cannot be clearly identified. For WC-FeCSiMn coating, it can be distinguished between the matrix material Fe, the inclusion FTC, and pores. Figure 6(a) shows an exemplary micrograph obtained from the coating.

An image processing tool is developed, which now identifies the phases and generates an image consisting of Fe- and W-based alloys and pores only. The differentiation between the phases is carried out by finding optimal thresholds based on the color distribution, from which the different phases are separated. As can be seen on the resulting image in Fig. 6(b), much noise and small single pieces of the material-phases are included, which make this image inappropriate to perform further analyses, especially with regard to plastic behavior. Therefore, these parts have to be smoothed out or removed by applying smoothing and cleanup algorithms. The resulting image is shown in Fig. 6(c).

To generate a FE-mesh from such an image, the software Object Oriented Finite Element 2 (OOF2), from the United States National Institute of Standards and Technology (NIST), is used. This software was developed to investigate the behavior of microstructures. OOF2 takes a non-reductionist approach to build a data structure on the digitized image of the microstructure whereby it gets connected to the associated material properties. At the end, OOF2 creates a FE-mesh which reflects the shape of the different phases in the microstructure with the associated material parameters. The mesh is generated by minimizing an energy functional E which is composed of a

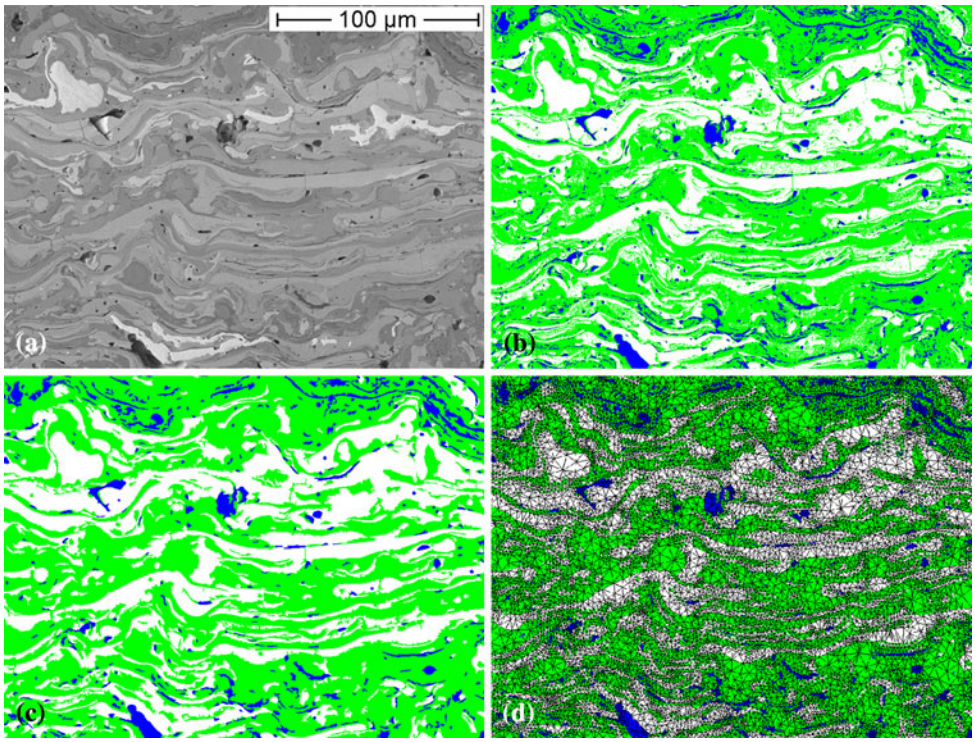

Fig. 6 (a) An exemplary micrograph obtained from a wire (AS-850) arc-sprayed coating with SEM. (b) Distinguished material phases. (c) Cleaned Image. (d) FE-mesh on microstructure

homogeneity part E_{hom} of the mesh and a shape part E_{shape} of the elements via

$$E = \alpha E_{hom} + (1 - \alpha) E_{shape}, \quad \text{(Eq 2)}$$

where α is an adjustable parameter, with which the user can control if the mesh should be highly accurate to the image with bad shaped elements ($\alpha = 1$) or if the elements are well shaped but with less accuracy to the shape of the phases in the micrograph ($\alpha = 0$). A value for α between these extremes will lead to an optimal choice. For further details about the exact formulation of the energy functional E and the features of the program OOF2, the readers are referred to Langer et al. (Ref 23) and Reid et al. (Ref 24). The resulting mesh can be seen in Fig. 6(d). The elements representing pores are removed by which free surfaces are created on which contact elements are applied to account for closing pores in the simulation. It is assumed that the phases are perfectly bonded.

To obtain information about the microstructural behavior and macroscopic properties, compression deformation tests are done. Because plane strain and plane stress conditions, respectively, would either over- or underestimate the lateral contraction which would lead to a too stiff or weak behavior, respectively, a 3D projection of the 2D mesh is performed by simple extrusion in normal direction of the mesh. At this point, it is crucial to investigate, how thick the model should be and how many layers are necessary over the thickness. Therefore, convergence studies are performed. It was found that a thickness of 100 µm by six layers gives an acceptable result.

The simple extrusion leads to columnar material phases which will still not predict the exact behavior but it is an improvement of a 2D simulation with plane strain or stress conditions. To receive more exact impressions of the microstructure, real 3D information of the coating would be necessary which are not available at this point. As boundary conditions for compression tests typical boundary conditions are chosen: three different lateral faces, which do not oppose each other, are fixed in their respective normal direction. The compression test is displacement controlled such that the displacement is applied to one of the free lateral sides in its respective normal direction. The simulations are performed using the Finite Element software ABAQUS. First tests are restricted to linear elasticity so that a comparison of the simulated with the predicted elastic constants from homogenization methods can be made. At this point, it is assumed that the micrographs fulfill the requirements for a Representative Volume Element. This is a crucial assumption to compare the obtained results with those from the homogenization methods. The elastic constants of the microstructure are obtained by evaluating the reaction forces at the boundaries and the displacement at the free lateral sides. The received results are presented in the next section.

4. Discussion

To receive macroscopic properties homogenization techniques can be used. The methods used are the Voigt, Reuss, and Hashin-Shtrinkman methods. These methods predict maximal and minimal bounds for the effective Young's modulus values with respect to the volume fraction of the two phases and pores. However, these methods do not take the morphology into account. Details to these methods can be found in Ref 25. The volume fractions were identified on the basis of the analyzed micrographs as mentioned in the previous section. The used volume fraction of FTC varies from 33.3 up to 36.6 vol.%, and for the pores from 0.72 to 2 vol.%, and the difference to make up 100 vol.% is used for FeCSiMn. The obtained results with these methods are compared to results from compression tests with real microstructures.

Owing to the lamellar structure of the coating (cp. Fig. 6a), it behaves anisotropic with respect to the normal (ND, perpendicular to the lamellar structure) and horizontal directions (HD, in direction of the lamellar structure) as was previously reported for coatings in Ref 8, 13. Therefore, the microstructure has to be tested with two different load directions, parallel and perpendicular to the lamellae. This procedure discussed in the previous section is performed on seven different micrographs created from the same part at different positions. The results of the calculated values of the effective Young's moduli are shown in Fig. 7. The effect of anisotropy is not accounted in the homogenization techniques because these methods assume homogenously distributed spherical inclusion and calculate the effective Young's modulus on the basis of the volume fractions. However, these methods provide a general impression about the values for the Young's modulus. The predicted Young's moduli obtained with help of the real microstructures do not violate the Voigt and Reuss bounds thus making the results valid. However, the effective Young's modulus does not lie between the Hashin-Shtrinkman bounds due to its anisotropy. It can be observed that the effective modulus calculated for the micrographs is slightly different because of the inhomogeneities of the coating. Therefore, the effective Young's

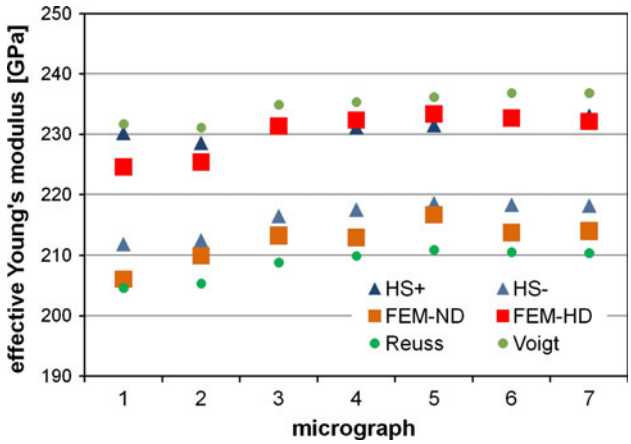

Fig. 7 Predicted effective Young's modulus calculated from real microstructures compared (HD = parallel to lamellar structure, ND = perpendicular to lamellar structure) with results from different homogenization techniques. (HS+ = upper Hashin-Shtrinkman bound, HS− = lower Hashin-Shtrinkman bound)

modulus has to be evaluated statistically over different micrographs. In this study, the resulting Young's moduli are calculated to be $E_{HD} = 230$ GPa and $E_{ND} = 212$ GPa.

Compared to the calculated averaged values in the experiment from all indents for an indentation depth of 100 nm ($E_{HD} = 240$ GPa (indentation in cross section) and $E_{ND} = 154$ GPa (indentation in surface), cp. Table 2), the predicted values fit for the horizontal direction. However, the averaged nanoindentation test results in normal direction do not agree with the predicted Young's modulus. One reason for this could be the local nature of nanoindentation tests. Due to the lamellar structure and relatively high aspect ratio of the lamellae and therefore small thickness in normal direction, the potential to indent a pore during nanoindentation tests in the surface without being visibly noticed is much higher than in the case of nanoindentation test in the cross section due to the high thickness in this direction. In contrast, the simulation determines the macro Young's modulus by such local phenomena that do not occur.

Considering the elasto-plastic material parameters of the two phases, both show very high yield stresses. The FTC phase shows a high rate of work hardening in which the saturation value is only 20% higher than the yield strength. It is anticipated that the FTC phase would break before hardening occurs. However, the investigated phases do not contain pure FTC. It is still a composite of not only FTC but also of other elements like Fe included in the wire. The FeCSiMn phase shows a more significant hardening behavior compared to the FTC phase. The yield stress is very high for Fe compared to conventional steels which will also depend on the included FTC. In summary, the single phases show very high mechanical properties although it is not possible to identify these for every chemical composition. Furthermore, it is typically assumed that the mechanical properties are inferior compared to bulk material. Although no bulk material is available of this composite, this assumption can be approved for the elastic region by comparing the results for the single phases with values from the literature (e.g., Ref 15). However, the plastic parameters are higher compared with those which might occur due to the high temperature during the thermal-spraying process, which leads to a hardening in the material phases.

From the above experiments, it is known that nearly no plastic deformation occurs in the coating. The coating fails at very low stress states, especially under tensile load (Ref 11). This can be attributed to the weak interface between the splats which leads to significantly poor mechanical properties compared to bulk materials. This means that the phases are not perfectly bonded to each other and that the interface fails. To include these effects and to model the coating more realistically, an interface model in conjunction with a failure model for the FTC phase has to be included. To do this, the interface as well as failure mechanisms in FTC have to be characterized in more detail in experiments which are part of on-going research. Therefore, we restricted the application of the calculation on basis of the real microstructure to linear elasticity; however, it can also be applied for the plastic region with the help of the identified parameters in Table 1 for the single phases. However, the computational time gets much larger because further effects just mentioned have to be included to get sensible results. The incorporation of an interface model is the part of the one-going research.

5. Summary and Outlook

TWAS-sprayed WC-FeCSiMn coatings have been evaluated with regard to their mechanical properties. In this article, the coating was investigated with regard to nanoindentation tests in detail. The analytic Oliver-Pharr method was used to determine the Young's modulus of local points. With SEM and EDX analysis, the material composites indented by the nanoindenter were identified. The elasto-plastic properties were obtained for each phase composition with simulation tools.

With help of an in-house image analysis software, different chemical compositions could be identified from SEM-micrographs. A method is presented generating FE-models on the basis of these images, which was successfully used to determine the global properties of the coating from the local properties of the single chemical compositions, which was presented for the elastic properties. These results were compared to the averaged experimental nanoindentation results as well as to results obtained by several analytical homogenization approaches. The obtained elastic properties in the simulation agree quite well with the averaged experimental values from all indents in the direction of the lamelar structure. However, the predicted values do not agree with the experimental measured Young's modulus in normal direction.

The presented method will be further developed to incorporate the interface between the single phases to model the global plastic behavior more realistically. Furthermore, the failure behavior of the coating will be investigated to enable us to predict cracks occurring in the coating during loading.

Acknowledgments

This study was supported by the German Research Foundation (DFG) within the SFB 708. Special thanks to R. Zarnetta (Institute of Materials, Ruhr University Bochum) for his support realizing the nanoindentation experiments. The authors thank the two reviewers for their annotations to improve the quality of this article.

References

1. Y. Santana, P. Renault, M. Sebastiani, J.L. Barbera, J. Lesage, E. Bemporad, E.L. Bourhis, E. Puchi-Cabrera, and M. Staia, Characterization and Residual Stresses of WC-Co Thermally Sprayed Coatings, *Surf. Coat. Technol.*, 2008, **202**(18), p 4560-4565
2. G. Pharr, W. Oliver, and F. Brotzen, On the Generality of the Relationship Among Contact Stiffness, Contact Area, and Elastic Modulus During Indentation, *J. Mater. Res.*, 1992, **7**(3), p 613-617

3. W. Oliver and G. Pharr, Improved Technique for Determining Hardness and Elastic Modulus Using Load and Displacement Sensing Indentation Experiments, *J. Mater. Res.*, 1992, **7**(6), p 1564-1580
4. R. Ghafouri-Azar, J. Mostaghimi, and S. Chandra, Modeling development of Residual Stresses in Thermal Spray Coatings, *Comput. Mater. Sci.*, 2006, **35**(1), p 13-26
5. M. Toparli, F. Sen, O. Culha, and E. Celik, Thermal Stress Analysis of HVOF Sprayed WC-Co/NiAl Multilayer Coatings on Stainless Steel Substrate Using Finite Element Methods, *J. Mater. Process. Technol.*, 2007, **190**(1-3), p 26-32
6. D. Delfosse, N. Cherradi, and B. Ilschner, Numerical and Experimental Determination of Residual Stresses in Graded Materials, *Composites, Part B*, 1997, **28**(1-2), p 127-141
7. I. Hussainova, J. Kubarsepp, and J. Pirso, Mechanical Properties and Features of Erosion of Cermets, *Wear of Materials*, 1st ed., R.G. Bayer and D.A. Rigney, Ed., April 22-26, 2001 (Vancouver), 2001, p 818-825
8. Z. Yin, S. Tao, X. Zhou, and C. Ding, Evaluating Bending Strength of Plasma Sprayed Al_2O_3 Coatings, *J. Therm. Spray Technol.*, 2009, **18**(2), p 292-296
9. H.P. Brantner, R. Pippan, and W. Prantl, Local and Global Fracture Toughness of a Flame Sprayed Molybdenum Coating, *J. Therm. Spray Technol.*, 2003, **12**(4), p 560-571
10. W. Tillmann, E. Vogli, I. Baumann, B. Krebs, and J. Nebel, Thermally Sprayed Wear-Protective Cermet Coatings for Forming Tools, *The 4th International Conference on Spray Deposition and Melt Atomization, SDMA 2009* (Bremen, Germany), 2009
11. J. Nebel, E. Vogli, and W. Tillmann, Arc spraying of WC-FeC-SiMn Cored Wires. Part 1: Bending, Compression, and Tension Behavior: Thermal Spray (ITSC), *Global Solutions for Future Applications*, May 3-5, 2010 (Singapore), 2010, p 607-615
12. W. Tillmann, E. Vogli, I. Baumann, B. Krebs, and J. Nebel, Wear-Protective Cermet Coatings for Forming Tools/Cermet-Schichten für den Verschleißschutz von Umformwerkzeugen, *Materialwiss. Werkstofftech*, 2010, **41**(7), p 597-607
13. H.-J. Kim and Y.-G. Kweon, Elastic Modulus of Plasma-Sprayed Coatings Determined by Indentation and Bend Tests, *Thin Solid Films*, 1999, **342**(1-2), p 201-206
14. R. W. Hertzberg, *Deformation and Fracture Mechanics of Engineering Materials*, 4th ed., John Wiley & Sons, Chichester, 1995, 816 p
15. S. Okamoto, Y. Nakazono, K. Otsuka, Y. Shimoitani, and J. Takada, Mechanical Properties of WC/Co Cemented Carbide with Larger WC Grain Size, *Mater. Charact.*, 2005, **55**(4-5), p 281-287
16. M. Dao, N. Chollacoop, K. Vliet, T. Venkatesh, and S. Suresh, Computational Modeling of the Forward and Reverse Problems in Instrumented Sharp Indentation, *Acta Mater.*, 2001, **49**(19), p 3899-3918
17. C.L. Hsieh and W.H. Tuan, Poisson's Ratio of Two-Phase Composites, *Mater. Sci. Eng. A*, 2005, **396**(1-2), p 202-205
18. A.E. Giannakopoulos and S. Suresh, Determination of Elastoplastic Properties by Instrumented Sharp Indentation, *Scripta Mater.*, 1999, **40**(10), p 1191-1198
19. T.A. Venkatesh, K.J.V. Vliet, A.E. Giannakopoulos, and S. Suresh, Determination of Elasto-Plastic Properties by Instrumented Sharp Indentation: Guidelines for Property Extraction, *Scripta Mater.*, 2000, **42**(9), p 833-839
20. Z. Shan and S.K. Sitaraman, Elastic-Plastic Characterization of Thin Films Using Nanoindentation Technique, *Thin Solid Films*, 2003, **437**(1-2), p 176-181
21. S. Kok and N. Stander, Optimization of a Sheet Metal Forming Process Using Successive Multipoint Approximations, *Struct. Optim.*, 1999, **18**(4), p 277-295
22. J.M. Lee, D.C. Ko, K.S. Lee, and B.M. Kim, Identification of the Bulk Behavior of Coatings by Nano-Indentation Test and FE-Analysis and Its Application to Forming Analysis of the Coated Steel Sheet, *J. Mater. Process. Technol.*, 2007, **187-188**, p 309-313
23. S.A. Langer, E.R. Fuller, and W.C. Carter, Oof: An Image-Based Finite-Element Analysis of Material Microstructures, *Comput. Sci. Eng.*, 2001, **3**(3), p 15-23
24. A.C. Reid, S.A. Langer, R.C. Lua, V.R. Coffman, S. Haan, and R.E. Garca, Image-Based Finite Element Mesh Construction for Material Microstructures, *Comput. Mater. Sci.*, 2008, **43**(4), p 989-999
25. S. Nemat-Nasser and M. Hori, *Micromechanics: Overall Properties of Heterogeneous Materials*, 2nd ed., Elsevier, 1999, 786 p